Evaluation of ^{111}In-DOTA-5D3, a Surrogate SPECT Imaging Agent for Radioimmunotherapy of Prostate-Specific Membrane Antigen

Sangeeta Ray Banerjee[1], Vivek Kumar[1], Ala Lisok[1], Donika Plyku[1], Zora Nováková[2], Mary Brummet[1], Bryan Wharram[1], Cyril Barinka[2], Robert Hobbs[1], and Martin G. Pomper[1]

[1]Department of Radiology and Radiological Science, Johns Hopkins Medical Institutions, Baltimore, Maryland; and [2]Institute of Biotechnology of the Czech Academy of Sciences, BIOCEV, Vestec, Czech Republic

5D3 is a new high-affinity murine monoclonal antibody specific for prostate-specific membrane antigen (PSMA). PSMA is a target for the imaging and therapy of prostate cancer. ^{111}In-labeled antibodies have been used as surrogates for ^{177}Lu/^{90}Y-labeled therapeutics. We characterized ^{111}In-DOTA-5D3 by SPECT/CT imaging, tissue biodistribution studies, and dosimetry. **Methods:** Radiolabeling, stability, cell uptake, and internalization of ^{111}In-DOTA-5D3 were performed by established techniques. Biodistribution and SPECT imaging were done on male nonobese diabetic/severe combined immunodeficient (NOD/SCID) mice bearing human PSMA(+) PC3 PIP and PSMA(−) PC3 flu prostate cancer xenografts on the upper right and left flanks, respectively, at 2, 24, 48, 72, and 192 h after injection. Biodistribution was also evaluated in tumor-free, healthy male CD-1 mice. Blocking studies were performed by coinjection of a 10-fold and 50-fold excess of 5D3 followed by biodistribution at 24 h to determine PSMA binding specificity. The absorbed radiation doses were calculated on the basis of murine biodistribution data, which were translated to a human adult man using organ weights as implemented in OLINDA/EXM. **Results:** ^{111}In-DOTA-5D3 was synthesized with specific activity of approximately 2.24 ± 0.74 MBq/μg (60.54 ± 20 μCi/μg). Distribution of ^{111}In-DOTA-5D3 in PSMA(+) PC3 PIP tumor peaked at 24 h after injection and remained high until 72 h. Uptake in normal tissues, including the blood, spleen, liver, heart, and lungs, was highest at 2 h after injection. Coinjection of ^{111}In-DOTA-5D3 with a 10- and 50-fold excess of nonradiolabeled antibody significantly reduced PSMA(+) PC3 PIP tumor and salivary gland uptake at 24 h but did not reduce uptake in kidneys and lacrimal glands. Significant clearance of ^{111}In-DOTA-5D3 from all organs occurred at 192 h. The highest radiation dose was received by the liver (0.5 mGy/MBq), followed by the spleen and kidneys. Absorbed radiation doses to the salivary and lacrimal glands and bone marrow were low. **Conclusion:** ^{111}In-DOTA-5D3 is a new radiolabeled antibody for imaging and a surrogate for therapy of malignant tissues expressing PSMA.

Key Words: SPECT/CT; PSMA; SPECT; immunoimaging; monoclonal antibody; prostate cancer

J Nucl Med 2019; 60:400–406
DOI: 10.2967/jnumed.118.214403

Prostate cancer (PC) is the most frequently diagnosed cancer and the second most common cause of cancer-related mortality in men in the United States (*1*). Prostate-specific membrane antigen (PSMA) is a well-characterized tumor marker associated with PC (*2–5*). Although PSMA expression is high in PC, including within metastases (*6–8*), it is also variably elevated in the neovasculature of solid tumors (*9–12*).

Small-molecule (≤1,000 Da) ligands targeting PSMA have proliferated for detecting, imaging, and treating PC (*4,13–16*). Many researchers worldwide currently focus on development of new and improved therapeutic PSMA small-molecule radioligands that deliver β- or α-particle–emitting payloads. Nevertheless, such agents are fraught with certain side effects, such as damage to salivary gland tissues (*17,18*). Renal toxicity may also emerge because more patients are treated more often and live longer (*19,20*). PSMA-targeted monoclonal antibodies (mAbs) have not been shown to accumulate significantly within off-target sites other than bone marrow, suggesting that mAbs may complement or be used in lower doses with lower doses of the small-molecule therapeutics.

PSMA-targeted mAbs have long been used to image and treat PC (*21*). The scintigraphy-based agent ^{111}In-7E11-356 was the first such agent approved by the Food and Drug Administration and is specific for an intracellular epitope of PSMA (*22*). Some have argued that those binding sites are exposed only after apoptosis or necrosis, suggesting the 7E11-356 scaffold to be suboptimal for clinical use (*23,24*). Bander's group subsequently developed the mAb huJ591, which targets an extracellular epitope of PSMA (*9,25–27*). Evaluation of ^{131}I- and ^{111}In-DOTA analogs of J591 demonstrated superior PSMA-specific tumor targeting and blood clearance compared with those based on 7E11-356 (*28*). More recently, a new mAb, 3/A12, which targets an external epitope different from that targeted by J591, was developed for immunoimaging (*29*). We characterized 4 new murine PSMA-specific mAbs, which we compared with J591 (*30*). We showed that mAb 5D3 binds to the external epitope of PSMA and at least partially overlaps with the J591 binding site but has 10-fold higher affinity. Here, we extend those results by synthesizing a ^{111}In-labeled analog of 5D3 and test its pharmacokinetics in vivo. ^{111}In was chosen not just for imaging with SPECT but also to

Received May 8, 2018; revision accepted Sep. 7, 2018.
For correspondence or reprints contact: Sangeeta Ray Banerjee, Johns Hopkins Medical Institutions, Cancer Research Building 2, 1550 Orleans St., Baltimore, MD 21287.
E-mail: sray9@jhmi.edu
Published online Sep. 20, 2018.

serve as a surrogate for other DOTA-chelated therapeutic nuclides, including ^{90}Y and ^{177}Lu for PSMA-based radiotherapeutics as a stand-alone agent and in combination with small-molecule radiotherapeutics.

MATERIALS AND METHODS

Reagents, Cell Lines, and Animal Models

5D3 (in phosphate-buffered saline and 0.01% NaN_3; 4.5 mg/mL; molecular weight, 150,000) was purified by the combination of protein-affinity chromatography and size-exclusion chromatography as described previously (*30*). Chemicals were purchased from Sigma-Aldrich or Fisher Scientific with 2 exceptions: DOTA-*N*-hydroxysuccinimide ester was purchased from Macrocyclics, and $^{111}InCl_3$ was purchased from Nordion. Sublines of the androgen-independent PC3 human PC cell line, originally derived from an advanced androgen-independent bone metastasis, were used. These sublines have been modified to express high levels of PSMA [PSMA-positive (+) PC3 PIP] or are devoid of target [PSMA-negative (−) PC3 flu] (*31*). LNCaP cells were purchased from American Type Culture Collection. Animal studies were performed in compliance with the regulations of the Johns Hopkins Animal Care and Use Committee. Six- to 8-wk-old male, nonobese diabetic/severe combined immunodeficient (NOD/SCID) mice (Johns Hopkins Animal Resources Core) were implanted subcutaneously with PSMA(+) PC3 PIP and PSMA(−) PC3 flu cells (2×10^6 in 100 μL of Matrigel [Corning]) at the forward right and left flanks, respectively. The mice were imaged or used in biodistribution assays when the xenografts reached about 5 mm in diameter.

Preparation of Radiolabeled ^{111}In-DOTA-5D3

5D3 was reacted with DOTA-*N*-hydroxysuccinimide-ester at a 1:10 (mAb:DOTA-*N*-hydroxysuccinimide-ester) molar ratio for 2 h at room temperature using 0.1 M sodium carbonate (pH 9) as the conjugating buffer followed by purification using centrifugal filter units (Thermo Scientific) and equilibrated with 0.2 M NH_4OAc (~pH 7.4). Conjugation of DOTA-*N*-hydroxysuccinimide-ester was confirmed by matrix-assisted laser desorption/ionization time-of-flight mass spectrometry. The resulting immuno–chelate conjugate, DOTA-5D3, was obtained in approximately 65% (n = 5) yield. DOTA-5D3 was radiolabeled with ^{111}In in 0.2 M NH_4OAc (~pH 4) for 1 h at 40°C. The resulting ^{111}In-DOTA-5D3 was incubated with ethylenediaminetetraacetic acid at a final concentration of 10 mM for 5 min to chelate unbound ^{111}In and then was subsequently purified on a phosphate-buffered saline preequilibrated Zeba spin desalting column (Thermo Scientific). Radiochemical purity and stability of ^{111}In-DOTA-5D3 were tested by instant thin-layer chromatography using ethylenediaminetetraacetic acid solution as a mobile phase. After purification, the overall purity was at least 98% starting from a crude purity of about 70%–80%. Protein concentration was determined using a NanoDrop spectrophotometer (Thermo Scientific).

Cell Uptake and Internalization, Immunoreactive Fraction, Flow Cytometry, and Immunohistochemistry

Experimental methods for cell culture, in vitro cell uptake and internalization studies, flow cytometry, and immunohistochemistry were performed following our previous report (*32,33*). The immunoreactive fraction of ^{111}In-DOTA-5D3 was determined by the Lindmo method (*34*).

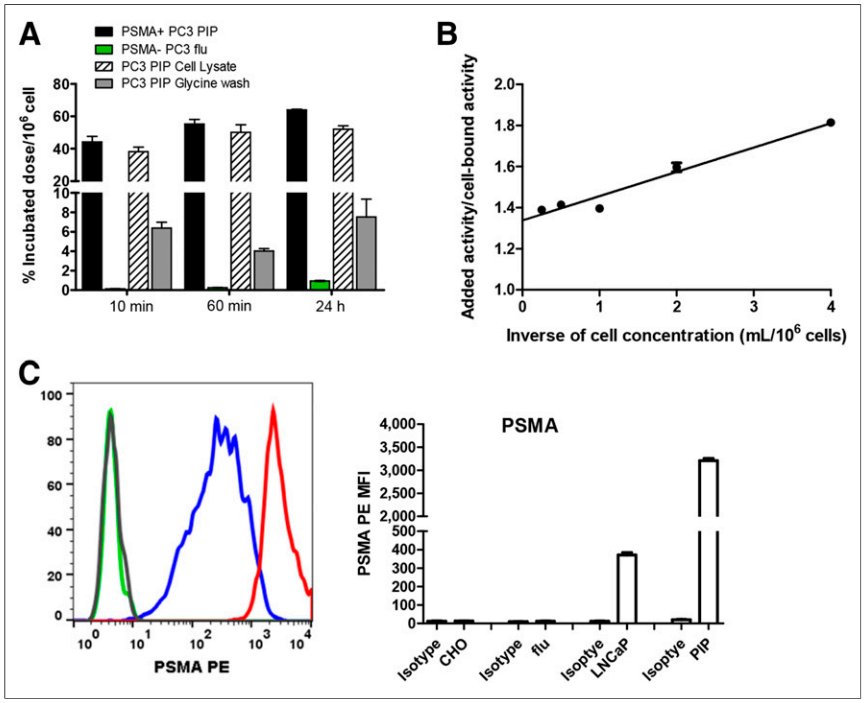

FIGURE 1. (A) In vitro binding specificity of ^{111}In-DOTA-5D3 in PSMA(+) PC3 PIP and PSMA(−) PC3 flu cell lines at 37°C. (B) Immunoreactive fractions of ^{111}In-DOTA-5D3 in PSMA(+) PC3 PIP cells was determined as 1/y (x = 0). (C) Cell surface PSMA expression by flow cytometry illustrated by overlapping histograms and mean fluorescence intensity (MFI) for 4 different cell lines: CHO (Chinese hampster ovary cell line with no staining with anti-PSMA mAb), PC3 flu (human PC3 with no staining with anti-PSMA mAb), PC3 PIP (human PC3 with PSMA-positive staining with anti-PSMA mAb), and LNCaP (human prostate cell line). Notice shift for no staining (CHO, gray; flu, green) and staining with PE antihuman PSMA (FOLH1) mAb (LNCaP, blue; PIP, red). PSMA PE = phycoerythrin (PE)-conjugated anti-PSMA antibody.

Biodistribution

Mice bearing PSMA(+) PC3 PIP and PSMA(−) PC3 flu xenografts were administered 0.37 MBq of ^{111}In-DOTA-5D3 (~10 μg) in 150 μL of saline (n = 4) via the tail vein. Additionally, we performed biodistribution studies with healthy immunocompetent CD-1 mice at 2 and 24 h using a similar dose. Competitive inhibition studies were performed in vivo using intact 5D3 (100 μg or 500 μg/mouse) added to the ^{111}In-DOTA-5D3 formulation, and biodistribution studies were performed at 24 h (n = 3).

SPECT/CT Imaging

SPECT/CT imaging of ^{111}In-DOTA-5D3 on a GammaMedica X-SPECT was used to study male NOD/SCID mice with tumor xenografts (n = 2) following a reported method (*31*). Data were reconstructed and fused using commercial software from the vendor (GammaMedica). Data were analyzed using AMIDE (http://amide.sourceforge.net/).

Radiation Dosimetry

Radiation doses absorbed by normal tissues and tumor were calculated for ^{111}In and ^{177}Lu, the latter of which is the initial candidate for therapy. Organ activity concentrations obtained from the murine biodistribution studies using ^{111}In-DOTA-5D3 were translated to human whole-organ percentage of injected dose and then integrated over time to obtain the human time-integrated activity coefficients, which were then input into OLINDA/EXM

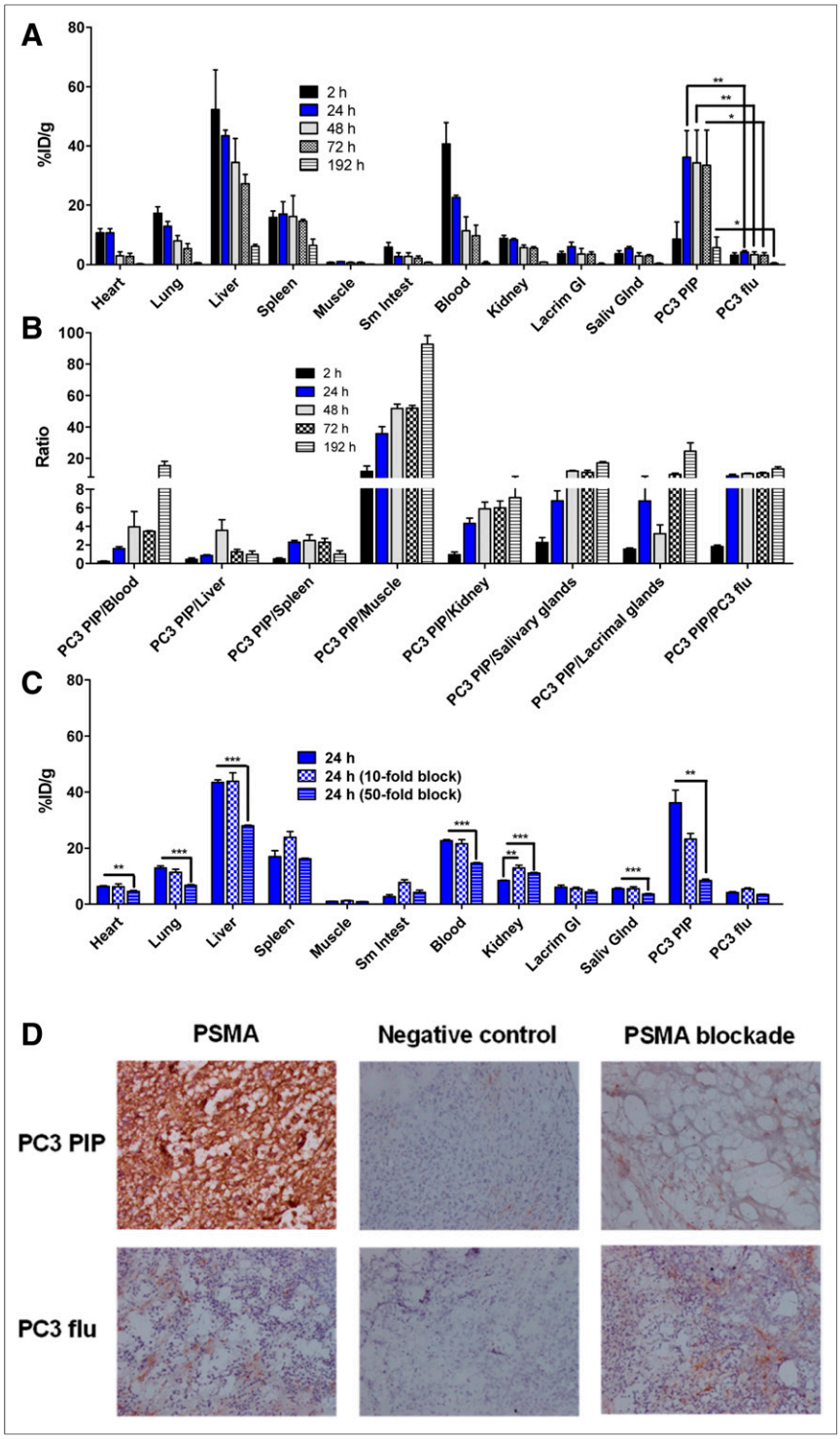

FIGURE 2. (A) Tissue biodistribution of ^{111}In-DOTA-5D3 in male NOD-SCID mice bearing PSMA(+) PC3 PIP and PSMA(−) PC3 flu tumors on either flank (n = 4). (B) Selected PSMA(+) PC3 PIP tumor-to-normal organ ratios. (C) Binding specificity assessed by blockade with coinjection of either 10- or 50-fold excess of nonradiolabeled 5D3. (D) Immunohistochemistry of PSMA expression and negative control (no PSMA staining) of frozen tissue sections of PSMA(+) PC3 PIP tumor and PSMA(−)PC3 flu tumor at ×10 magnification obtained from biodistribution experiment at 24 h after injection of ^{111}In-DOTA-5D3 and from blocking experiment at 24 h using 50-fold excess of 5D3.

software to obtain the organ-absorbed doses (*35*). The activity concentration in human red marrow was estimated using a previously described method (*36*). Previously developed Monte Carlo–based models were used to estimate the doses absorbed by the salivary and lacrimal glands following our previous report (*37*). The related equations, explanations, and assumptions for dosimetry calculations are available on request.

Statistical Analysis

Statistical analysis was performed using a 2-tailed t test (GraphPad). P values were considered significant if they were 0.05 or less.

RESULTS

Radiolabeling of ^{111}In-DOTA-5D3

5D3 was first conjugated with DOTA-mono-*N*-hydroxysuccinimide ester following the scheme in Supplemental Figure 1 (supplemental materials are available at http://jnm.snmjournals.org). Conjugation and purification chemistry proceeded in an approximately 65% yield with high chemical purity (≥98%) to generate DOTA-5D3. Mass spectrometry confirmed conjugation of an average of 2 molecules of the chelator for each antibody (Supplemental Fig. 2). The final radiochemical yield of the purified DOTA-5D3 was about 60% ± 10%, with radiochemical purity of more than 98% and a specific activity of 2.24 ± 0.74 MBq/μg (60.54 ± 20 μCi/μg). Incubation of ^{111}In-DOTA-5D3 in phosphate-buffered saline for 7 d at 37°C revealed a less than 2% decrease in radiochemical purity.

PSMA-Specific Cell Uptake and Internalization

^{111}In-DOTA-5D3 displayed rapid uptake in PSMA(+) PC3 PIP cells at 37°C within 10 min after incubation (44.27% ± 1.99%) (Fig. 1; Supplemental Table 1). A relatively slow but steady increase in cell uptake was observed over time at 30 min (49.04% ± 1.38%) and 1 h (55.29% ± 1.65%) and held at that level for 24 h. Cell internalization of ^{111}In-DOTA-5D3 was rapid, with 38.23% ± 1.65% of the dose internalized at 10 min and 50.23% ± 2.72% at 1 h. Those values remained steady at 24 h. Uptake of ^{111}In-DOTA-5D3 in LNCaP cells (Supplemental Table 2) was significantly lower at 30 min (14.45% ± 0.40%) and 1 h after incubation (23.37% ± 0.80%) than in PSMA(+) PC3 PIP cells. However, at 24 h after incubation, ^{111}In-DOTA-5D3 demonstrated comparable uptake (50.71% ± 0.65% in LNCaP vs. 54.64% ± 1.12% in PSMA(+) PC3 PIP). Control experiments

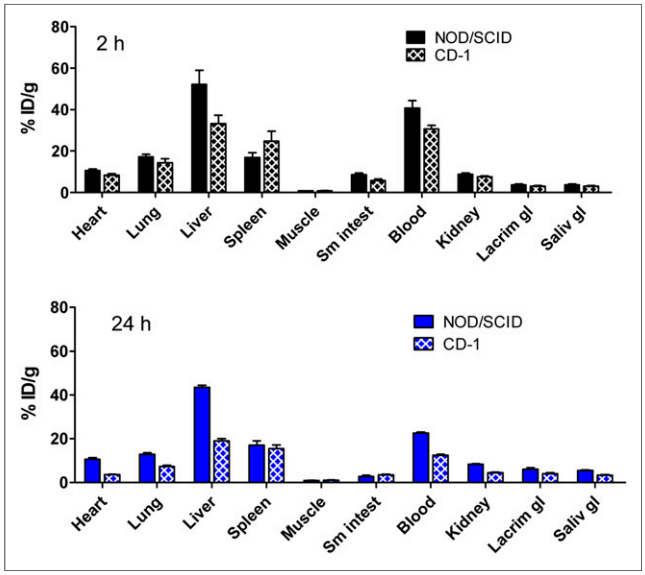

FIGURE 3. Biodistribution analysis at 2 h and 24 h after injection of ^{111}In-DOTA-5D3 in male NOD-SCID bearing PSMA(+) PC3 PIP and PSMA(−) PC3 flu tumors on either flank (n = 4) and in male CD-1 mice (n = 3).

using the PSMA(−) PC3 flu cells showed no specific binding up to 24 h after incubation, further demonstrating the specificity of ^{111}In-DOTA-5D3. Cell surface expression of PSMA in those 3 cell lines was evaluated by flow cytometry (Fig. 1C). The PSMA(+) PC3 PIP cell line displayed approximately 10-fold higher PSMA expression than LNCaP. The control PSMA(−) PC3 flu cell line displayed significantly lower expression than PSMA(+) PC3 PIP or LNCaP cells. The immunoreactive fraction of ^{111}In-DOTA-5D3 was about 75% ± 6% (Fig. 1B).

PSMA-Specific Tumor Uptake and Biodistribution Studies

At 2 h after injection, ^{111}In-DOTA-5D3 uptake was mainly in the blood (40.70 ± 7.16 percentage injected dose per gram [%ID/g]), liver (52.26 ± 13.43 %ID/g), and spleen (16.99 ± 4.18 %ID/g) (Figs. 2A and 2B; Supplemental Table 3). On the basis of mono-exponential clearance of blood time–activity curves, the half-life of blood clearance of ^{111}In-DOTA-5D3 was 29.2 h (Supplemental Fig. 3). PSMA(+) PC3 PIP tumor uptake at 2 h was 5.72 ± 0.87 %ID/g. PSMA(+) PC3 PIP tumor uptake was high at 24 h after injection (36.19 ± 9.00 %ID/g), remained nearly at that level through 48 and 72 h, and significantly decreased to 5.77 ± 3.53 % ID/g at 192 h. High PC3 PIP tumor accumulation of ^{111}In-DOTA-5D3 is consistent with prolonged blood-pool activity (24 h, 22.62 ± 0.75 %ID/g; 48 h, 11.39 ± 4.68 %ID/g; and 72 h, 9.74 ± 3.62 %ID/g) and rapid cellular internalization and sequestration of the complex. Uptake in the PSMA(−) PC3 flu tumors was significantly lower at all time points tested ($P < 0.05$, paired 2-tailed t test; Supplemental Fig. 4). The ratio of PSMA(+) to PSMA(−) tumor uptake was about 1.87 at 2 h and remain high (>5) after 24 h to 8 d after administration.

Competitive inhibition (blocking) studies were performed in vivo by coinjection of ^{111}In-DOTA-5D3 with a 10-fold (100 μg) and 50-fold (500 μg) excess of nonradiolabeled mAb (Fig. 2C; Supplemental Table 4; Supplemental Fig. 5) at 24 h after injection. Decreased tissue binding was observed for the 50-fold blockade. Most normal tissue uptake decreased on blockade; however, kidney uptake increased to 11.04 ± 0.26 %ID/g ($P < 0.0005$ relative to unblocked). Blocking with a 10-fold excess of nonradiolabeled mAb also resulted in increased uptake in the kidneys (12.96 ± 0.92 %ID/g) compared with unblocked ^{111}In-DOTA-5D3. Uptake in the PSMA(+) PC3 PIP tumor was not significantly reduced compared with unblocked ^{111}In-DOTA-5D3 (23.20 ± 3.56 %ID/g with the 10-fold blockade; $P = 0.07$ relative to unblocked). However, nearly 4-fold lower tumor uptake (8.45 ± 0.53 %ID/g) was observed using 50-fold blockade. Although lacrimal gland uptake did not show any significant change with either 10-fold or 50-fold blockade, salivary glands showed significantly reduced uptake at the higher dose ($P < 0.005$ relative to unblocked). No significant changes in radiolabeled mAb were observed within spleen, muscle, bone, small intestine, or PSMA(−) PC3 flu tumor using the 50-fold blockade. Low nonspecific uptake in the PSMA(−) PC3 flu tumor was most likely associated with the enhanced permeability and retention effect of DOTA-5D3. The competitive inhibition experiments demonstrate the high specificity of ^{111}In-DOTA-5D3 for PSMA expression in vivo.

Immunohistochemistry of the frozen tissue sections of PSMA(+) PC3 PIP and PSMA(−) PC3 flu tumors—those that were unblocked and those subjected to 50-fold blockade—at 24 h is shown in Figure 2D. Significant reduction of PSMA-positive staining was found in the blocked PSMA(+) PC3 PIP tumor tissue sections compared with the unblocked tumor sections, in agreement with blocking data shown in Figure 2C. PSMA(−) PC3 flu cells did not show any change in PSMA staining, as expected.

We have also performed tissue biodistribution studies of ^{111}In-DOTA-5D3 in immunocompetent healthy CD-1 mice at 2 and 24 h after injection and compared the results with those for the tumor-bearing NOD/SCID mice (Fig. 3). In the immunocompetent CD-1 mice, ^{111}In-DOTA-5D3 demonstrated a biodistribution pattern similar to that in the tumor-bearing mice, except for the organs noted below. Liver (18.97 ± 1.81 %ID/g), kidney (4.55 ± 0.11 %ID/g), and blood (12.51 ± 0.58 %ID/g) uptake in the CD-1 mice at 24 h were nearly 2-fold lower than in the tumor-bearing NOD/SCID mice ($P < 0.0001$).

In Vivo SPECT Imaging

Whole-body SPECT/CT images depicting the biodistribution of ^{111}In-DOTA-5D3 at 2, 24, 48, 72, and 192 h after injection are presented in Figure 4. At 2 h, signal intensity was highest in the liver, spleen, and gallbladder, and signal was also observed in the region of the spinal column. The signal intensity within the spinal column likely reflects the high concentration of ^{111}In-DOTA-5D3 in the circulation. From 24 to 72 h after injection, clearance of ^{111}In-DOTA-5D3 from nontarget tissues, including the blood and

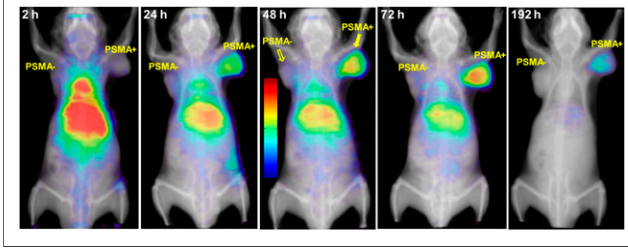

FIGURE 4. Whole-body volume rendering SPECT/CT images in male NOD-SCID mice showing uptake of ^{111}In-DOTA-5D3 in normal tissues (e.g., liver, kidneys) and PSMA(+) PC3 PIP and PSMA(−) PC3 flu tumors.

liver, allowed visualization of PSMA(+) PC3 PIP tumor. Relative to 2 h, the radioactivity concentration within the liver was reduced, whereas the signal intensity persisted in the PSMA(+) PC3 PIP tumor for up to 8 d.

Organ-Absorbed Doses

Figure 5 and Supplemental Tables 6 (*37–39*) and 7 provide a selected list of the human organ time-integrated activity coefficients (h) and absorbed doses (mGy/MBq), respectively, for ^{111}In and ^{177}Lu. For both isotopes, the liver received the highest absorbed dose per unit activity, as expected from the biodistribution study. Accordingly, it is likely that the liver would be the dose-limiting organ, followed by the spleen. The absorbed doses of ^{177}Lu for the kidneys, lacrimal glands, parotid glands, and submandibular glands were low, within the range 0.10–0.17 mGy/MBq, whereas the liver dose was 0.97 mGy/MBq. The estimated bone marrow dose for both ^{111}In-DOTA-5D3 and ^{177}Lu-DOTA-5D3 was low, 0.04 mGy/MBq.

DISCUSSION

We previously reported that 5D3 was suitable for the development of radioimmunotherapy targeting PSMA-expressing malignancies (*30*). This study examined the in vitro properties and in vivo pharmacokinetics and binding specificity of ^{111}In-DOTA-5D3, which enabled SPECT imaging of PSMA-expressing xenografts (Fig. 4). 5D3 may also allow the development of new radiopharmaceutical therapies—or antibody–drug conjugates—for the treatment of PSMA-expressing tumors. High tumor uptake and retention of ^{111}In-DOTA-5D3 are most likely related to high internalization of the radiometal-labeled mAb within the tumor, resulting in metabolism and trapping of the radioactivity at the tumor site (*40*). Accordingly, we anticipate that the longer-lived therapeutic radionuclide, ^{177}Lu (maximum β^-, 0.497 MeV; half-life, 6.74 d), will have longer in situ tumor irradiation than will ^{90}Y (maximum β^-, 2.28 MeV; half-life, 2.67 d).

For most radioimmunotherapeutic agents, the critical organ is the red marrow (*41*). Although liver and spleen demonstrated the highest absorbed dose for ^{111}In-/^{177}Lu-DOTA-J591, the major concern for ^{177}Lu-DOTA-J591 is myelotoxicity for a therapeutically effective dose (*42,43*). Our biodistribution data suggest that clearance of ^{111}In-DOTA-5D3 from tumor-bearing NOD/SCID mice and healthy immunocompetent CD-1 mice is slightly faster than that of ^{111}In-DOTA-J591, whereas uptake in the liver and spleen has been shown to be more than 3-fold higher for ^{111}In-DOTA-5D3 than for ^{111}In-DOTA-J591 after 48 h (*28*). As a result, the estimated human red marrow absorbed dose of ^{177}Lu-DOTA-5D3 (0.04 mGy/MBq), was slightly lower than that of ^{177}Lu-DOTA-J591 (0.3 ± 0.1 mGy/MBq) (*43*). Although we recognize that such a comparison may not be appropriate based on the preclinical data, consideration of the liver–to–red-marrow absorbed dose ratio of ^{177}Lu-DOTA-J591 and ^{177}Lu-DOTA-5D3 (6 vs. 24) further suggests that the liver might be the dose-limiting organ for ^{177}Lu-DOTA-5D3.

Salivary gland radiotoxicity is presently a major impediment for more widespread use of PSMA-targeted α-particle therapy (*17*), although various off-target tissue-blocking strategies are currently being developed (*18*). Salivary gland uptake of ^{111}In-DOTA-5D3 could be significantly blocked with a 50-fold excess of unlabeled mAb 5D3, indicating that the uptake of ^{111}In-DOTA-5D3 in the salivary glands is at least in part mediated by PSMA. This possibility is also supported by immunohistochemistry (Supplemental Fig. 6). Although ^{177}Lu-DOTA-J591 did not display any salivary gland radiotoxicity, and there is no preclinical report of salivary gland uptake, we anticipate that the mAb ^{111}In/^{177}Lu-DOTA-5D3 will similarly not deliver a high radiation dose to the salivary glands. The estimated dose absorbed by the salivary glands, 0.24 mGy/MBq, is much lower than the estimated dose from ^{177}Lu-PSMA-617, 1.4 mGy/MBq (*44*). Additionally, the absorbed dose within the lacrimal glands for ^{111}Lu-DOTA-5D3 (0.12 mGy/MBq) was significantly lower than that of ^{177}Lu-PSMA-617 (2.82 mGy/MBq) (*45*).

Anticipating and mitigating off-target effects is critical for implementing new radiopharmaceutical therapeutics. Increased kidney uptake observed using 2 different blocking doses indicated that kidney uptake of ^{111}In-DOTA-J591 was mostly due to clearance of the mAb and not to PSMA expression in the kidney (Supplemental Fig. 6). PSMA-based small-molecule agents developed by us and others demonstrate significant renal cortical blocking using competitive, small-molecule blockers (*46,47*), underscoring differences in pharmacokinetics between PSMA-based mAbs and low-molecular-weight agents.

The largely nonoverlapping off-target effects of ^{111}In-DOTA-5D3, which would

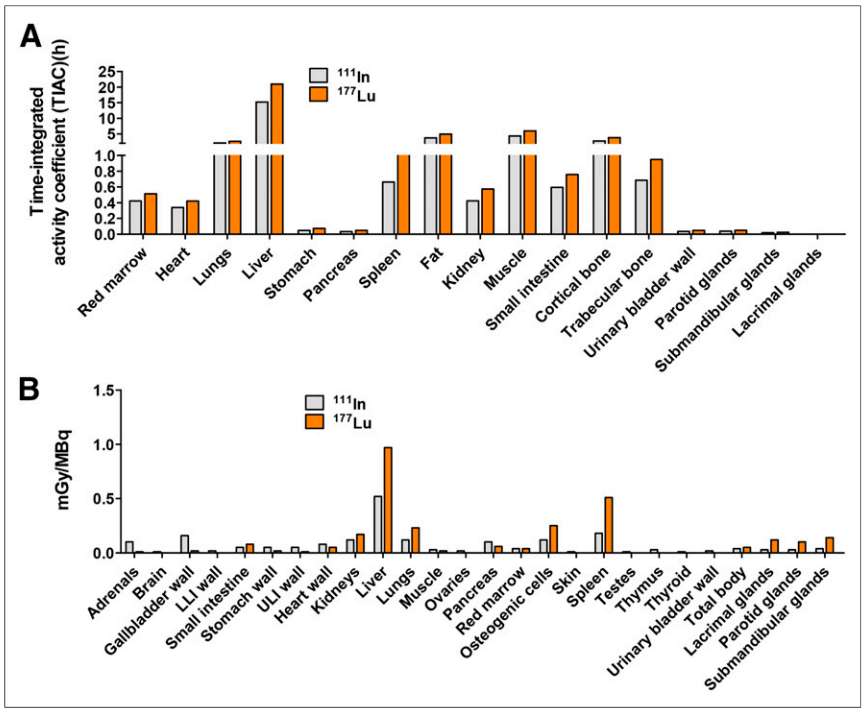

FIGURE 5. (A) Calculated human organ time-integrated activity coefficients. (B) Estimated human organ absorbed doses (mGy/MBq). Absorbed doses were calculated on the basis of murine biodistribution data, which were converted into adult human absorbed doses. Calculated time-integrated activities were used as input in OLINDA/EXM using adult male phantom for normal tissues.

likely be similar for the corresponding ^{177}Lu analog and the small-molecule PSMA agents such as ^{177}Lu-PSMA-617, may enable their use in tandem or together, with a concurrent decrease in the dose of each—perhaps sparing marrow and salivary and lacrimal gland tissue, respectively. According to the report of a recent meeting organized by the Prostate Cancer Foundation, "Simultaneous administration of radiolabeled small molecules targeting PSMA and PSMA-targeted antibodies are non-competitive and. . .dual administration leads to additive dose to tumor" (Bander et al., unpublished) (*48*). Significantly, the approach is currently being attempted with combination of ^{177}Lu-J591 and ^{177}Lu-PSMA-617 in patients with metastatic castration-resistant PC (NCT03545165). Although it is difficult to predict the therapeutic index for human subjects on the basis of preclinical studies, the ^{111}In-DOTA-5D3 biodistribution studies here also justify preclinical radioimmunotherapeutic studies with ^{177}Lu/^{90}Y radionuclides with a tolerable marrow radiation dose.

CONCLUSION

Biodistribution and immuno-SPECT experiments indicate that ^{111}In-DOTA-5D3 demonstrates high potential as a radionuclide-based agent for specific, noninvasive delineation of PSMA-expressing tissues, particularly PC, in vivo. ^{111}In-DOTA-5D3 also serves as a template on which to build PSMA-targeted radiotherapeutics.

DISCLOSURE

Financial support was provided by the Patrick Walsh Foundation, the Commonwealth Foundation, the National Institutes of Health (EB024495), the Czech Science Foundation (18-04790S), the Czech Academy of Sciences (86652036), and the European Regional Development Fund (CZ.1.05/1.1.00/02.0109). No other potential conflict of interest relevant to this article was reported.

REFERENCES

1. Prostate cancer. Centers for Disease Control and Prevention website. https://www.cdc.gov/cancer/prostate/basic_info/what-is-prostate-cancer.htm. Updated June 7, 2018. Accessed November 1, 2018.
2. Chang SS. Overview of prostate-specific membrane antigen. *Rev Urol.* 2004; 6(suppl):S13–S18.
3. Bouchelouche K, Choyke PL, Capala J. Prostate specific membrane antigen: a target for imaging and therapy with radionuclides. *Discov Med.* 2010;9:55–61.
4. Kiess AP, Banerjee SR, Mease RC, et al. Prostate-specific membrane antigen as a target for cancer imaging and therapy. *Q J Nucl Med Mol Imaging.* 2015; 59:241–268.
5. Haberkorn U, Eder M, Kopka K, Babich JW, Eisenhut M. New strategies in prostate cancer: prostate-specific membrane antigen (PSMA) ligands for diagnosis and therapy. *Clin Cancer Res.* 2016;22:9–15.
6. Sweat SD, Pacelli A, Murphy GP, Bostwick DG. Prostate-specific membrane antigen expression is greatest in prostate adenocarcinoma and lymph node metastases. *Urology.* 1998;52:637–640.
7. Silver DA, Pellicer I, Fair WR, Heston WD, Cordon-Cardo C. Prostate-specific membrane antigen expression in normal and malignant human tissues. *Clin Cancer Res.* 1997;3:81–85.
8. Haffner MC, Laimer J, Chaux A, et al. High expression of prostate-specific membrane antigen in the tumor-associated neo-vasculature is associated with worse prognosis in squamous cell carcinoma of the oral cavity. *Mod Pathol.* 2012;25:1079–1085.
9. Liu H, Moy P, Kim S, et al. Monoclonal antibodies to the extracellular domain of prostate-specific membrane antigen also react with tumor vascular endothelium. *Cancer Res.* 1997;57:3629–3634.
10. Chang SS, O'Keefe DS, Bacich DJ, Reuter VE, Heston WD, Gaudin PB. Prostate-specific membrane antigen is produced in tumor-associated neovasculature. *Clin Cancer Res.* 1999;5:2674–2681.
11. Milowsky MI, Nanus DM, Kostakoglu L, et al. Vascular targeted therapy with anti–prostate-specific membrane antigen monoclonal antibody J591 in advanced solid tumors. *J Clin Oncol.* 2007;25:540–547.
12. Spatz S, Tolkach Y, Jung K, et al. Comprehensive evaluation of prostate specific membrane antigen expression in the vasculature of renal tumors: implications for imaging studies and prognostic role. *J Urol.* 2018;199:370–377.
13. Morris MJ, Vogelzang NJ, Sartor O, et al. Phase 1 study of the PSMA-targeted small-molecule drug conjugate EC1169 in patients with metastatic castrate-resistant prostate cancer (mCRPC) [abstract]. *J Clin Oncol.* 2017;35(suppl):5038.
14. Afshar-Oromieh A, Holland-Letz T, Giesel FL, et al. Diagnostic performance of ^{68}Ga-PSMA-11 (HBED-CC) PET/CT in patients with recurrent prostate cancer: evaluation in 1007 patients. *Eur J Nucl Med Mol Imaging.* 2017;44: 1258–1268.
15. Rahbar K, Ahmadzadehfar H, Kratochwil C, et al. German multicenter study investigating ^{177}Lu-PSMA-617 radioligand therapy in advanced prostate cancer patients. *J Nucl Med.* 2017;58:85–90.
16. Perera M, Papa N, Christidis D, et al. Sensitivity, specificity, and predictors of positive ^{68}Ga–prostate-specific membrane antigen positron emission tomography in advanced prostate cancer: a systematic review and meta-analysis. *Eur Urol.* 2016;70:926–937.
17. Kratochwil C, Bruchertseifer F, Rathke H, et al. Targeted alpha-therapy of metastatic castration-resistant prostate cancer with ^{225}Ac-PSMA-617: dosimetry estimate and empiric dose finding. *J Nucl Med.* 2017;58:1624–1631.
18. Taïeb D, Foletti JM, Bardies M, Rocchi P, Hicks RJ, Haberkorn U. PSMA-targeted radionuclide therapy and salivary gland toxicity: why does it matter? *J Nucl Med.* 2018;59:747–748.
19. Schwartz J, Jaggi JS, O'Donoghue JA, et al. Renal uptake of bismuth-213 and its contribution to kidney radiation dose following administration of actinium-225-labeled antibody. *Phys Med Biol.* 2011;56:721–733.
20. Erbas B, Tuncel M. Renal function assessment during peptide receptor radionuclide therapy. *Semin Nucl Med.* 2016;46:462–478.
21. Elsässer-Beile U, Buhler P, Wolf P. Targeted therapies for prostate cancer against the prostate specific membrane antigen. *Curr Drug Targets.* 2009;10: 118–125.
22. Horoszewicz JS, Kawinski E, Murphy GP. Monoclonal antibodies to a new antigenic marker in epithelial prostatic cells and serum of prostatic cancer patients. *Anticancer Res.* 1987;7:927–935.
23. Troyer JK, Feng Q, Beckett ML, Wright GL. Biochemical characterization and mapping of the 7E11-C5.3 epitope of the prostate-specific membrane antigen. *Urol Oncol.* 1995;1:29–37.
24. Troyer JK, Beckett ML, Wright GL Jr. Location of prostate-specific membrane antigen in the LNCaP prostate carcinoma cell line. *Prostate.* 1997;30: 232–242.
25. Vallabhajosula S, Kuji I, Hamacher KA, et al. Pharmacokinetics and biodistribution of ^{111}In- and ^{177}Lu-labeled J591 antibody specific for prostate-specific membrane antigen: prediction of ^{90}Y-J591 radiation dosimetry based on ^{111}In or ^{177}Lu? *J Nucl Med.* 2005;46:634–641.
26. Tagawa ST, Milowsky MI, Morris M, et al. Phase II study of lutetium-177-labeled anti-prostate-specific membrane antigen monoclonal antibody J591 for metastatic castration-resistant prostate cancer. *Clin Cancer Res.* 2013;19:5182–5191.
27. Pandit-Taskar N, O'Donoghue JA, Divgi CR, et al. Indium-111-labeled J591 anti-PSMA antibody for vascular targeted imaging in progressive solid tumors. *EJNMMI Res.* 2015;5:28.
28. Smith-Jones PM, Vallabhajosula S, Navarro V, Bastidas D, Goldsmith SJ, Bander NH. Radiolabeled monoclonal antibodies specific to the extracellular domain of prostate-specific membrane antigen: preclinical studies in nude mice bearing LNCaP human prostate tumor. *J Nucl Med.* 2003;44:610–617.
29. Elsässer-Beile U, Reischl G, Wiehr S, et al. PET imaging of prostate cancer xenografts with a highly specific antibody against the prostate-specific membrane antigen. *J Nucl Med.* 2009;50:606–611.
30. Nováková Z, Foss CA, Copeland BT, et al. Novel monoclonal antibodies recognizing human prostate-specific membrane antigen (PSMA) as research and theranostic tools. *Prostate.* 2017;77:749–764.
31. Banerjee SR, Pullambhatla M, Byun Y, et al. Sequential SPECT and optical imaging of experimental models of prostate cancer with a dual modality inhibitor of the prostate-specific membrane antigen. *Angew Chem Int Ed Engl.* 2011;50: 9167–9170.
32. Ray Banerjee S, Chen Z, Pullambhatla M, Mease RC, Pomper MG. A preclinical comparative study of ^{68}Ga-labeled DOTA, NOTA and HBED-CC chelated radiotracers for targeting PSMA. *Bioconjug Chem.* 2016;27:1447–1455.
33. Banerjee SR, Foss CA, Horhota A, et al. ^{111}In- and IRDye800CW-labeled PLA-PEG nanoparticle for imaging prostate-specific membrane antigen-expressing tissues. *Biomacromolecules.* 2017;18:201–209.
34. Konishi S, Hamacher K, Vallabhajosula S, et al. Determination of immunoreactive fraction of radiolabeled monoclonal antibodies: what is an appropriate method? *Cancer Biother Radiopharm.* 2004;19:706–715.

35. Stabin MG, Sparks RB, Crowe E. OLINDA/EXM: the second-generation personal computer software for internal dose assessment in nuclear medicine. *J Nucl Med.* 2005;46:1023–1027.
36. Sgouros G. Bone marrow dosimetry for radioimmunotherapy: theoretical considerations. *J Nucl Med.* 1993;34:689–694.
37. Plyku D, Mena E, Rowe SP, et al. Combined model-based and patient-specific dosimetry for ^{18}F-DCFPyL, a PSMA-targeted PET agent. *Eur J Nucl Med Mol Imaging.* 2018;45:989–998.
38. ICRP. Publication 89: basic anatomical and physiological data for use in radiological protection reference values. *Ann ICRP.* 2002;32:3–4.
39. Snyder WS, Cook MJ, Nasset ES, Karhausen LR, Howells GP, Tipton IH. *ICRP Publication 23: Report of the Task Group on Reference Man.* Elmsford, NY: International Commission on Radiological Protection; 1975.
40. Wu AM, Senter PD. Arming antibodies: prospects and challenges for immunoconjugates. *Nat Biotechnol.* 2005;23:1137–1146.
41. Behr TM, Sgouros G, Vougioukas V, et al. Therapeutic efficacy and dose-limiting toxicity of auger-electron vs. beta emitters in radioimmunotherapy with internalizing antibodies: evaluation of ^{125}I- vs. ^{131}I-labeled CO17-1A in a human colorectal cancer model. *Int J Cancer.* 1998;76:738–748.
42. Vallabhajosula S, Goldsmith SJ, Kostakoglu L, Milowsky MI, Nanus DM, Bander NH. Radioimmunotherapy of prostate cancer using ^{90}Y- and ^{177}Lu-labeled J591 monoclonal antibodies: effect of multiple treatments on myelotoxicity. *Clin Cancer Res.* 2005;11:7195s–7200s.
43. Vallabhajosula S, Goldsmith SJ, Hamacher KA, et al. Prediction of myelotoxicity based on bone marrow radiation-absorbed dose: radioimmunotherapy studies using ^{90}Y- and ^{177}Lu-labeled J591 antibodies specific for prostate-specific membrane antigen. *J Nucl Med.* 2005;46:850–858.
44. Delker A, Fendler WP, Kratochwil C, et al. Dosimetry for ^{177}Lu-DKFZ-PSMA-617: a new radiopharmaceutical for the treatment of metastatic prostate cancer. *Eur J Nucl Med Mol Imaging.* 2016;43:42–51.
45. Hohberg M, Eschner W, Schmidt M, et al. Lacrimal glands may represent organs at risk for radionuclide therapy of prostate cancer with [^{177}Lu]DKFZ-PSMA-617. *Mol Imaging Biol.* 2016;18:437–445.
46. Kratochwil C, Giesel FL, Leotta K, et al. PMPA for nephroprotection in PSMA-targeted radionuclide therapy of prostate cancer. *J Nucl Med.* 2015;56:293–298.
47. Banerjee SR, Foss CA, Pullambhatla M, et al. Preclinical evaluation of ^{86}Y-labeled inhibitors of prostate-specific membrane antigen for dosimetry estimates. *J Nucl Med.* 2015;56:628–634.
48. Miyahira AK, Pienta KJ, Morris MJ, et al. Meeting report from the Prostate Cancer Foundation PSMA-directed radionuclide scientific working group. *Prostate.* 2018;78:775–789.

The Journal of NUCLEAR MEDICINE

Evaluation of ^{111}In-DOTA-5D3, a Surrogate SPECT Imaging Agent for Radioimmunotherapy of Prostate-Specific Membrane Antigen

Sangeeta Ray Banerjee, Vivek Kumar, Ala Lisok, Donika Plyku, Zora Nováková, Mary Brummet, Bryan Wharram, Cyril Barinka, Robert Hobbs and Martin G. Pomper

J Nucl Med. 2019;60:400-406.
Published online: September 20, 2018.
Doi: 10.2967/jnumed.118.214403

The Journal of Nuclear Medicine is published monthly.
SNMMI | Society of Nuclear Medicine and Molecular Imaging
1850 Samuel Morse Drive, Reston, VA 20190.
(Print ISSN: 0161-5505, Online ISSN: 2159-662X)

SNMMI SOCIETY OF NUCLEAR MEDICINE AND MOLECULAR IMAGING